Comparison of model potentials for molecular dynamics simulations of silica

Daniel Herzbach and Kurt Binder

Institut für Physik, WA 331, Universität Mainz, 55099 Mainz, Germany

Martin H. Müser

Department of Applied Mathematics, University of Western Ontario, London, Ontario N6A 5B7, Canada
(Dated: March 27, 2005)

Structural, thermomechanical, and dynamic properties of pure silica, SiO_2, are calculated with three different model potentials, namely the potential suggested by van Beest, Kramer, and van Santen (BKS), the fluctuating charge potential with a Morse stretch term for the short-range interactions proposed by Demiralp, Cagin, and Goddard (DCG), Phys. Rev. Lett. **82**, 1708 (1999), and a polarizable force field proposed by Tangney and Scandolo (TS), J. Chem. Phys. **117**, 8898 (2002). The DCG potential had to be modified due to flaws in the original treatment. While BKS reproduces many thermomechanical properties of different polymorphs rather accurately, it also shows qualitatively wrong trends concerning the phononic density of states, an absence of the experimentally observed anomaly in the c/a ratio at the quartz $\alpha - \beta$ transition, pathological instabilities in the β-cristobalite phase and a vastly overestimated transition pressure for the stishovite i - ii transition. These shortcomings are only partially remedied by the modified DCG potential but greatly improved by the TS potential. DCG and TS both reproduce a pressure-induced transition from α-quartz to quartz II, predicted theoretically based on the BKS potential.

I. INTRODUCTION

Understanding the thermomechanical properties of glassy silica and its various crystalline polymorphs has been subject of intensive research. [1] The interest in silica and silicates is due to their abundance in nature, their numerous technological applications, and their peculiar behavior that is challenging to understand. Good model potentials are required that describe the relevant atomic interactions in silicates if one wants to model and ultimately understand the properties of silicates from an atomistic point of view. In a pioneering work by Woodcock et al., [2] the energy surface of bulk SiO_2 systems was modeled as a sum over two-body potentials having the Born-Mayer-Huggins form. This interatomic pair potential was later generalized and parametrized by Tsuneyuki et al. based on ab initio Hartree-Fock self-consistent-field calculations. [3] The form of their potential, referred to as TTAM potential, is

$$\phi_{ij}(r) = \phi_{ij}^{\text{Coulomb}}(r) + A_{ij}e^{-B_{ij}r} - C_{ij}/r^6, \quad (1)$$

which consists of Coulomb interactions, Born-Mayer-type repulsion, and dispersive interactions. Van Beest, Kramer, and van Santen (BKS) reparametrized this model potential by combining microscopic (ab initio computations) and macroscopic (experimental) data. [4]

Both TTAM and BKS potential allow one to imitate thermomechanical properties of various silica polymorphs fairly well. In general, experimental findings are reflected slightly better with BKS than with TTAM. Yet, the use of the TTAM potential resulted in a respectable reproduction of the lattice parameters, bond lengths, and bulk modulus of α-quartz, α-cristobalite, coesite, and stishovite [3] as well as in a rather precise location of the α-β transition temperature of quartz at ambient pressures. [5] Pair correlation functions for α-

and β-cristobalite have been predicted using TTAM potentials [6] and later been found to be in good agreement with neutron scattering data. [7] Beside the original applications of the BKS potential to the properties of quartz, [4] crystalline-to-amorphous phase transitions, [8–10] and the equation of state for α-quartz, cristobalite, and stishovite [11, 12] were found to be in excellent agreement with experiment. Furthermore, predictions for the stability of various polymorphs under large uniform pressures were made [11, 13] and confirmed by experiment and first-principle calculations. [14] This confirmation is surprising, because the BKS potential had been optimized for four-coordinated silicon, while the high-pressure phases of silica consist of six-coordinated silicon. Also, ab initio calculations [15] supported molecular dynamics simulations [16] which predicted a transformation from α-quartz to five-coordinated silica polymorphs for certain non-uniform pressures. Moreover, the BKS potential was used rather successfully for the study of static and dynamic properties of molten and amorphous SiO_2. [17–22]

Despite the success of TTAM and BKS, some features remain unsatisfactory. This does not only concern their limited transferability to more generalized chemical compositions and/or to surface phenomena, but it also concerns bulk properties of *pure* SiO_2 in the bulk. For instance, the anomaly in the c/a ratio at the $\alpha - \beta$ transition in quartz is absent in molecular-dynamics (MD) simulations. [23] Moreover, the phononic density of states shows the wrong trend in the glassy phase [24] at small and intermediate frequencies, and as shown in this paper, BKS (as well as TTAM) β-cristobalite and tridymite are not thermodynamically stable: In order for these phases to appear stable in simulations, appropriate periodic boundary conditions must be chosen, i.e., boundary condition which are incommensurate with the modes

leading into the energetically favored structures.

Recently, a Morse stretched potential allowing for fluctuating charges was suggested by Demiralp, Cagin, and Goddard. [25] Fluctuating charge energy surfaces promise to be more easily transferable than rigid ion potentials, because the charges on individual atoms can adjust to the instantaneous chemical environment. A second approach, suggested by Tangney and Scandolo [26] adds a polarizability to the oxygen atoms, which introduces additional electrostatic interactions between the charges and the new dipoles. The polarizability of the oxygen atom is well established [27, 28] and is thus likely to mimic necessary electronic degrees of freedom.

While both groups of authors claimed their potential to mirror experimental observations rather well, none of their simulations addressed one of the above-mentioned points, where BKS and TTAM fail. It is thus necessary to check whether the two model potential approaches are able to remedy these failures.

The initial purpose of this study was to test the merits of the fluctuating charge model and the fluctuating dipole model for silica more thoroughly than this had been done before. However, as we will describe in more detail in the main part of this article, we had to realize soon that the treatment in the original paper proposing the fluctuating charge force field is flawed and that their data could not be reproduced. This does not imply that a fluctuating charge model has to fail per se, however, it was necessary to modify the pseudo potential of the fluctuating charge model in order to make a meaningful comparison to experimental SiO_2 systems. In the remainder of this paper, we will first give a brief overview over the methodology. This includes a discussion of the DCG and TS potential. In Sect. III, we test whether the DCG and TS potentials are able to reduce the discrepancies between experiments and ab initio simulations on one hand and classical force fields on the other hand. Sect. IV gives a summary.

II. METHOD AND MODELS

A. MD Methods

In this study, standard MD techniques are used. Constant temperature of the ionic motion is maintained via a Langevin thermostat and stress is kept constant within the Parrinello-Rahman method, similarly as described previously. [23] For the simulations allowing fluctuating charges, see below for more details, we used an extended Lagrange method. Both charge motion and ionic motion were damped with coefficients γ_q and γ_{ion}, respectively, but only ions experience random forces imposing nonzero temperatures. Time steps dt and the total simulation time t_s were chosen such that the following series of inequality held sufficiently well for our purposes:

$$dt \ll \frac{1}{w_q} \ll \frac{1}{\gamma_q} \ll \frac{1}{\omega_{ion}} \ll \frac{1}{\gamma_{ion}} \ll t_s, \qquad (2)$$

where ω_q and ω_{ion} are characteristic frequencies of the charge and the ionic motion. With these inequalities, it is ensured that the charges relax close to their equilibrium values for a given ionic configuration. At the same time, neither ionic nor charge motion is overdamped. We tested explicitly convergence of our results by changing the free parameters $dt = 0.1$ fs, $\omega_q \approx \mathcal{O}(3\,\text{fs})$ (adjusted by the choice of the charge inertia), $\gamma_q = 10$ fs, $\gamma_{ion} = 0.1$ ps, and t_s typically 10 ps, while the intrinsic frequency related to tetrahedral vibrations $\omega_{ion} = \mathcal{O}(30\,\text{fs})$.

With this choice of parameters, we see our results (lattice constants, elastic constants, DOS, internal energy, etc.) converged, that is to say, none of the observables' thermal averages changes within our (small) statistical error bars, if one of the free parameters is changed by a factor of two. The only exception is the DOS at small frequencies, where characteristic features such as peaks are slightly broadened due to the damping/thermostating related to ionic motion.

1. Implementation of the DCG potential

As mentioned above, fluctuating charge potentials allow the effective ionic charge on an atom to vary as a function of the local environment. Thus, at a given set of coordinates, the charges have to be determined first, before the forces on the ions can be determined. Often, the $1/r$ Coulomb potential is replaced with a function $J(r)$ in which the singularity at small distances is screened. For more information, we refer to the original literature. [29]

Despite careful implementation of the fluctuating-charge Morse stretched potential suggested by Demiralp, Cagin, and Goddard (DCG), we were not able to reproduce any data presented in Ref. 25, as long as we proceeded as described in the original publication. The original paper claims that the $1/r$ Coulomb potential is replaced by the smoothed $J(r)$ function. Using $J(r)$ for the charge optimization and the calculation of the forces did not enable us to reproduce any of the original results. We are yet confident about our implementation of the code, because we could most easily reproduce data on TiO_2 [30, 31], which was simulated with a model potential identical in form as that claimed to have been used by CGS.

Also replacing $J(r)$ back with the Coulomb potential did not remedy the situation. We could only reproduce the data published in Ref. 25 by using the $1/r$ potential for the calculation of the ionic forces, while the charges were optimized with respect to the $J(r)$ interaction (plus the additional term in a fluctuating charge potential such as the atomic hardness). While this treatment provides well-defined forces as a function of the coordinates, it is certainly unsatisfactory to treat charges and ions inconsistently. In particular, if the charges are not determined by exact diagonalisation but with an extended Lagrangian approach, it is not possible to check for energy conservation as charges and center of masses see a dif-
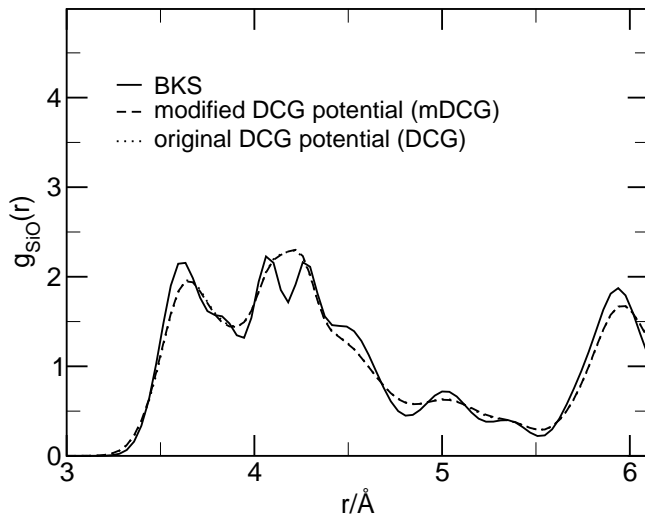
FIG. 1: Pair radial distribution function $g_{\mathrm{SiO}}(R)$ of α-quartz at 300 K. The curves for the new consistent fluctuating charge potential and the original inconsistent potential basically lie on top of each other. The nearest neighbor peak, which is located at 1.6 Å, is not included in the graph.

ferent potential energy surface. Therefore modifications needed to be applied, which are explained in the next section.

2. Modification of the DCG potential

In the following, we attempted to treat ionic and electronic potentials on equal grounds. It appears that the fit of the ab-initio data was based on the above-mentioned inconsistent treatment, as this was the only way to reflect the data published in the original paper. To obtain a consistent energy surface, we decided to use $J(r)$ for the electrostatic part (relevant to the charge equilibration) and to add a term $\langle q_i \rangle \langle q_j \rangle [J(r) - 1/r]$ (with $\langle q_i \rangle$ the average charge of ion i in α-quartz at ambient conditions) to the short range potential term. This modification is of course purely heuristically. However, it results in reasonably accurate partial radial distribution functions in α-quartz, and it also reproduces very well results from the inconsistent treatment, which had been fitted to first-principle calculations. All results presented in this paper were obtained in very close agreement with both the modified potential in an extended Lagrangian formalism and the original inconsistent approach with direct diagonalization. In the following we will refer to this modification as the mDCG potential.

B. TS potential

In the potential suggested by Tangney and Scandolo (TS), ionic charges are kept fixed, but the oxygen atoms

are polarizable. [26] The potential consists of a pair potential

$$U_{ij} = \frac{q_i q_j}{R_{ij}} + D_{ij}[e^{\gamma_{ij}(1-r_{ij}/r_{ij}^0)} - 2e^{\gamma_{ij}/2(1-r_{ij}/r_{ij}^0)}]. \quad (3)$$

with additional dipole moments on the oxygen atoms, which are calculated self consistently with the electric field in every MD step. The dipoles will interact electrostatically with the other dipoles in the system as well as with the charges, which are both calculated via Ewald summation. Following Wilson and Madden, [32] we include the effect of charge distribution overlap at short distances. A force routine provided by Paul Tangney was used for the TS potential.

III. RESULTS

A. Density of states in α-quartz

The vibrational density of states (DOS) is compared for the different models, in order to obtain an estimate for their accuracy of the lattice dynamics. The DOS, $g(\nu)$, gives the normalized number of eigenstates in the frequency range ν and $\nu + d\nu$. It was shown recently by first-principle calculations [24] that BKS does not reproduce the DOS of amorphous silica well, even though the BKS structures turned out to be quite accurate. In a large frequency range the nature of the excitations as determined by the BKS potential differed significantly from the one determined by ab initio methods. It is questionable whether other effective force fields improve the situation. It has been suggested that good agreement can (only) be found by employing shell models, which was shown for the phonon dispersion curves of α-quartz by Schober et al. [33]
Our calculations of the DOS were done at sufficiently small temperatures where the harmonic approximation is applicable. The DOS was determined by calculating the Fourier transform of the mass-weighted velocity autocorrelation function:

$$g(\nu) = \frac{1}{N k_B T} \sum_j m_j \int\limits_{-\infty}^{\infty} dt \, \langle \vec{v}_j(t).\vec{v}_j(0) \rangle \, e^{i2\pi\nu t}. \quad (4)$$

The most obvious disagreement between the lattice dynamics of a BKS simulation and an ab initio simulation can already be seen directly in the vibrational DOS in Fig. 2. The figure shows the DOS for α-quartz at 300 K with ab initio data from Roma et al., [34] which was chosen because no experimental measurement of the DOS in quartz could be found. The figure reveals that the inter-tetrahedral motions, the so-called rigid-unit modes, which account for the lower frequency vibrations, show a significant discrepancy between experiment and BKS. This has already been known for amorphous systems [24]. In the higher frequency range, the double peak structure
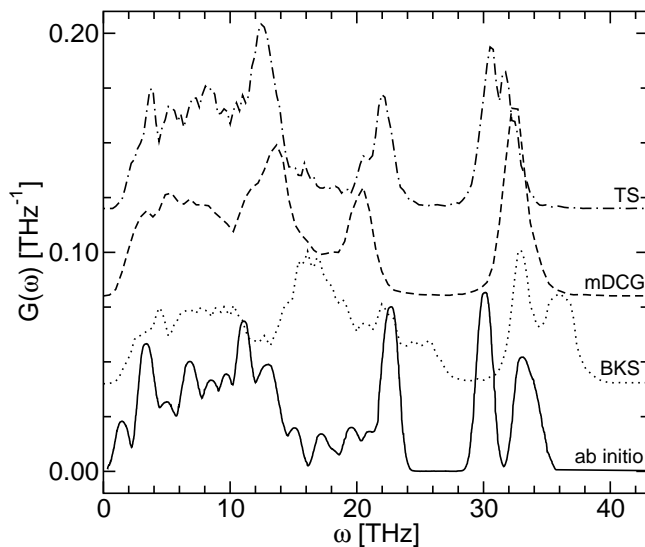
FIG. 2: Phonon Density of States in α-quartz at 300K. Comparison of BKS, mDCG, TS, and ab initio data. For clarity the curves for BKS, mDCG and TS have been shifted upwards.

is due to intra-tetrahedral stretching vibrations. [35, 36] The four oxygen atoms in an SiO_4 tetrahedron move at the higher frequency ("breathing mode") as compared to the central Si atom. At the lower frequency, two O-Atoms oscillate in anti-phase to each other. The frequency of these low-frequency tetrahedral oscillations to be shifted from 32.1 THz in vitreous silica as determined by vitreous silica [37] to around 30 THz in α-quartz as determined by ab initio calculations. The lower peak of the BKS potential, which coincides with the experimental frequency quite well, is shifted rather to a higher frequency of about 33 THz in α-quartz.

The fluctuating charge model coincides slightly better with ab initio at the lower frequencies. The experimentally observed peaks at 11 THz and 22 THz are reasonably well reproduced and the overall functional form of $g(\nu)$ is similar to the experimentally measured curve. The two peaks of the intra tetrahedral modes collapse on just a single peak, but exist at roughly the right frequency.

The best overall agreement for both the rigid unit modes and the double peak is clearly shown by the fluctuating dipole potential. This is not too surprising as it was parametrized to match ab initio forces and stresses. The fluctuating dipole potential almost coincides with the ab initio result in this case, only the tetrahedral breathing mode is slightly shifted in frequency.

While we mainly focus on properties which are not very well described by BKS, we also examined the elastic properties of the three potentials as a function of temperature. BKS was fitted to the elastic properties of α-quartz at room temperature, so that temperature-dependence of the elastic constants can be seen as an additional, partly independent test for BKS. Some rep-

	C_{11}	C_{33}	C_{44}	C_{66}	C_{12}	C_{13}
expt.	133.7	122.7	37.4	51.4	29.9	48.0
BKS	144.6	130.3	37.8	52.3	40.6	59.6
mDCG	108.3	108.1	37.9	37.8	23.8	43.0
TS	143.9	128.7	42.1	49.8	45.6	59.7

TABLE I: Elastic constants of β quartz at 1050 K in GPa. Experimental data (expt.) from Ref. 38, taken from Fig. 9
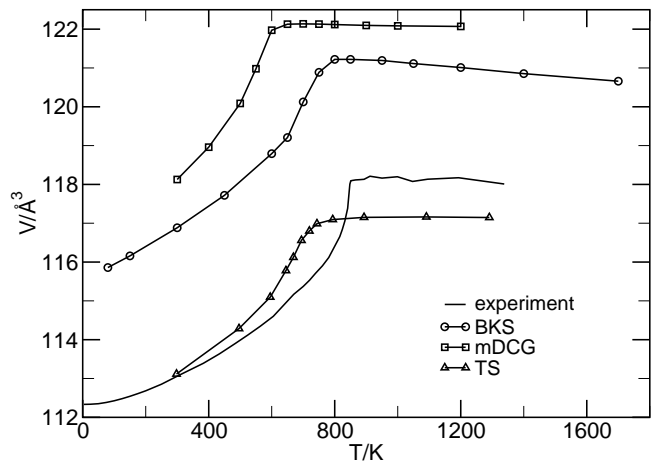

FIG. 3: Temperature dependence of the volume per unit cell at the α-β transition. All of the three different model potentials show qualitative agreement with experiment. The quantitative agreement is best for the TS potential.

resentative results at temperature $T = 1050$ K are listed in table I. It turns out that all three potentials reproduce the listed values within a reasonable standard variance, i.e., 7.0 GPa (BKS), 8.3 GPa (TS), and 11.3 GPa (mDCG). Thus, this comparison does not discriminate qualitatively between the three potentials.

B. The c/a anomaly at the α-β transition

The transition from α- to β-quartz is a displacive phase transition, which occurs at a transition temperature of $T_{tr} = 846$ K. The transition temperature in BKS is 740 K and turned out to be 712 K in TS and 581 K in mDCG. Obviously all three potentials underestimate the transition temperature. The discrepancy is most significant for the mDCG approach. For the determination of the phase transition temperature, we proceeded similarly as in Ref. 23, i.e., the fourth-order cumulant was evaluated for different system sizes [39] and the Landau expansion coefficients were determined at finite system size.

An important test for the different models is the temperature dependence of the volume close to the transition. As can be seen in Fig. 3, the BKS potential coincides fairly well with experiment, even though the volume is slightly overestimated and the transition temperature slightly underestimated as described in the previous section. The
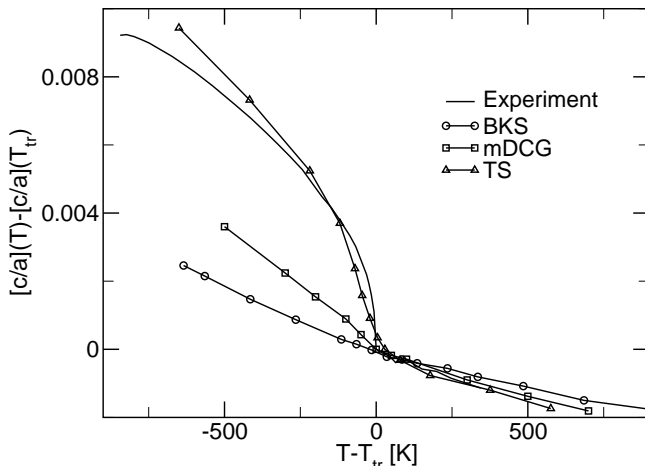
FIG. 4: Temperature dependence of the c/a ratio at the α-β transition. For easier comparison the curves are shifted to match at their respective transition temperature.

FIG. 5: Structures of α-quartz (top row) and β-quartz (bottom row) with dipoles from TS potential. Positions and dipoles are shown in a snapshot (left column) and in an averaged configuration (right column). Projection along the [100] direction, [001] direction is vertical.

result of the mDCG potential is quite similar, although the volume of both quartz phases is even bigger for this potential. The best quantitative agreement with experiment can be seen for the fluc-μ potential. The rather smooth behavior at the transition is due to the fact that the system sizes were so small that they allowed for the existence of both of the two phases in a quite broad temperature range around the transition.

The expansion at the transition is non-isotropic. A jump was observed experimentally [38] to be of different magnitude for different spatial directions, i.e., the ratio of the lattice constants c and a show a discontinuity at the transition. It was pointed out recently [23] that this discontinuity of the c/a ratio is absent in simulations based on the BKS potential. This is shown in figure 4 together with similar data for the mDCG and the TS potential. The mDCG potential has a change in the slope at the transition temperature. Thus there is at least an effect of the transition in the c/a ratio, but it is still far away from reproducing the experimental curve. In contrast, the TS approach matches the experimental course of the c/a ratio quite well. The relatively smooth behavior at the transition is again owing to the broad range of phase coexistence as discussed above.

A closer look at the origin of these differences can be done by investigating the influence of the fluctuating charges and the fluctuating dipoles on this behavior. If we use the fluctuating charge potential with the charges fixed on the average charges in α-quartz, the behavior of the c/a ratio is only marginally different. The kink at T_{tr} is still of the same shape as with fluctuating charges. In general, there is not much difference between the average charges in α-quartz, which are about $\langle Q_{\mathrm{Si}} \rangle = 1.318e$ for Si, and in β-quartz, where the value is $\langle Q_{\mathrm{Si}} \rangle = 1.293e$. So it is justified to state that the fluctuations of the charges barely affect the simulation, at least the kink in the c/a ratio is certainly not a result of *fluctuating* charges but
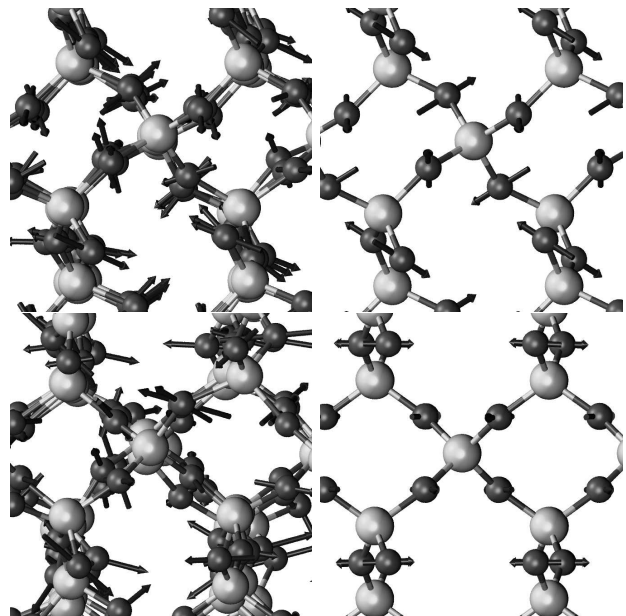
rather an effect of the pure two-body forces in the potential.

The same analysis for the fluctuating dipole potential results in a different picture. The simulation crucially depends on the fluctuating dipoles. When the dipoles are constrained to the average values found in α-quartz, the crystal would not transform to the β phase even at temperatures as high as $1300K$. Similarly, with fixed average β quartz dipoles the crystal would stay in a β-quartz configuration even at $300K$.

This shows that the dipoles (or the interactions parametrized as dipole interactions) contribute a major part of the thermodynamic driving force. The dipole configuration in α- and β-quartz is shown in Fig. 5 for a random snapshot and for the averaged values. The latter show the qualitative difference between the two phases: while the average of the z-direction (vertical) is symmetry forbidden in β-quartz, this component exists in the average α-quartz dipoles and drives the transition.

The physical origin for the behavior of the c/a ratio in quartz was investigated by Grimm and Dorner [40] and Smith [41]. They showed that while most observation associated with the transition can be explained by a simple tilting of rigid SiO_4 tetrahedra, this cannot explain the anomaly in the c/a ratio. Instead, it turned out to be directly related to the deformation in the tetrahedra. The shearing of the tetrahedra in the quartz phase is also well established experimentally. [38, 40, 42] To test if such a deformation is present in the simulations, one can investigate the angles $\vartheta_{\mathrm{OSiO}}$ formed by the silicon atoms with their four neighboring oxygen atoms, which

	Exp.	BKS	mDCG	TS
O_1-Si-O_2	110.5	107.5	108.6	110.1
O_1-Si-O_6	108.9	114.8	111.9	108.9
O_1-Si-O_5	108.8	108.2	108.8	109.1
O_2-Si-O_5	109.3	110.5	109.8	109.5

TABLE II: Bonding angles on the silicon atoms, experiment [42] versus model potentials.

is done in table II. The comparison shows the angles around the Si_1 position in α-quartz at $298K$, see the experimental paper by Kihara [42] for the definition of the numbering. Table II shows that the deviation between the ideal tetrahedral angle of 109.47 degrees and the calculated angles has the correct sign and amplitude for the fluctuating-dipole potential as compared with experiment, in contrast to the BKS result. One can see that the large deformation, that was also seen in the figures above, is actually much too large compared to experiment. Moreover, in three out of the four angles shown, the aberration from the tetraeder angle that is predicted by BKS has the wrong sign. Quantitatively, the root-mean-square deviations between model potential and experiment are 3.3 degrees (BKS), 1.8 degrees (mDCG), and 0.3 degrees (TS).

C. Pressure induced quartz I↔II transition

The high-pressure behavior of α-quartz is not yet fully understood neither theoretically nor experimentally. Tse et al. [43] suggested a phase transformation into a crystal of space group C2. For a recent discussion, we refer to Ref. 44. The majority of polymorphs that are observed at ambient to moderate pressures, such as cristobalite and quartz as well as other polymorphs including tridymite and coesite, are built up of SiO_4 tetrahedra. [1] At higher pressures dense forms containing SiO_6 octahedra are observed such as stishovite above 9 GPa, which has a rutile type structure. Because of the relatively strong Si-O bonding in silica, there are high kinetic barriers associated with the transitions to stable phases containing octahedrally coordinated silica at high pressure.

As the pressure is increased, the four-coordinated structures become increasingly unfavorable and eventually the polymorph becomes unstable. For molecular dynamics simulations employing the BKS potential it was shown that a phase transition occurs, when α-quartz is compressed to pressures above 22 GPa. [8, 11, 43] It is crucial for the transition to occur that a constant pressure regime with a fluctuating box geometry is used, as the new phase can only be established from the α-quartz configuration when the box is allowed to shear. The density changes in a compression/decompression cycle are shown in the equation of state in Fig. 6. Starting with the α-quartz configuration at zero pressure, the pressure is increased up to 21 GPa, where the system collapses from
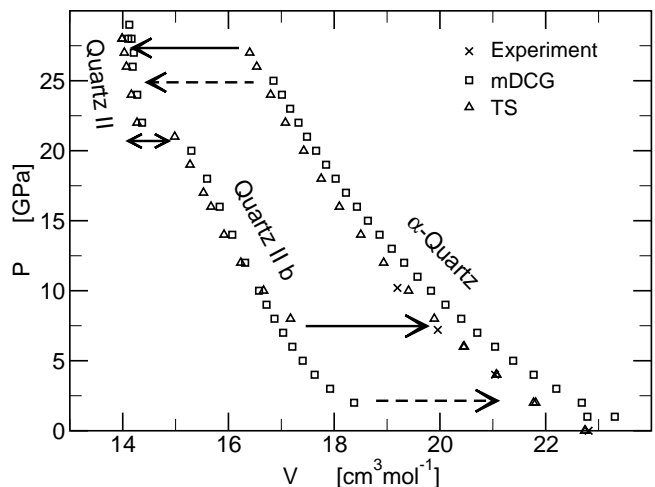

FIG. 6: Equation of state for α-quartz under pressure for mDCG and TS. Experiment and BKS both undergo the transition near 22 GPa. [44]

the α-quartz configuration into the quartz II phase. The transition is discontinuous in the volume and the new phase remains stable upon further compression and due to large hysteresis even on decompression below the transition pressure. The BKS behavior, which differs qualitatively on decompression from the two potentials shown here, can be seen in Fig. 1 in Ref. 44 For the mDCG and TS potentials the equation of state for different quartz phases is shown in Fig. 6. The phase transition in mDCG occurs, compared to BKS, at a slightly higher pressure of 25 GPa, and the volume of both the α-quartz and the quartz II phase agree very well with the BKS results. Nevertheless, the quartz II phase does not remain stable upon decompression, but the system undergoes a reversible phase transition at 21 GPa to a structurally similar phase named quartz II b in the figure. This phase has a smaller density than the BKS quartz II phase at the same pressure and reverts to the α-quartz phase at 4 GPa. These findings for the mDCG potential are also valid for TS. As shown in the same figure, the variation of the volume with pressure is identical to mDCG with respect to its qualitative features. The transition temperature to quartz II is 27 GPa for TS, and it has to be noted that the transition only occurs for small systems. For larger systems the α-quartz configuration is stabilized for even higher pressures. The transition to quartz II b occurs also at 21 GPa and the transition back to α-quartz will not take place until 2 GPa.

The similar behavior of the three model potentials at the quartz II transition. The apparent similarity of the crystalline structure emerging from these simulations gives the simulations a certain credibility for predictions towards experiment. In experiments, the structure of a crystal can be characterized by its diffraction pattern, such as by the energy dispersive x-ray diffraction spectra [45]. In simulations the structure factor can be calculated as well, and the resulting Bragg spacings can be
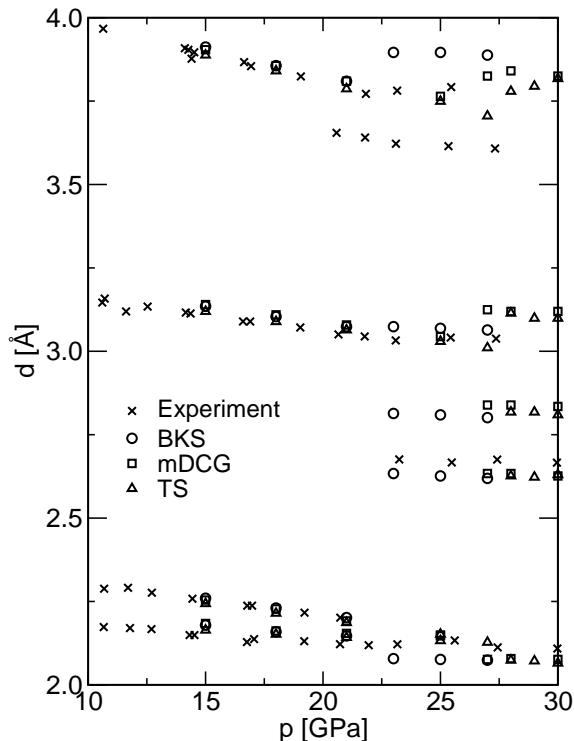
FIG. 7: Interplanar spacing for the compression of α-quartz in experiment and simulation. Experimental data by Kingma et al. [45]

read from the peak positions. In Fig. 7 the calculated interplanar spacings are shown and compared to the experimental data. It can be summarized that the features of the experimental spectrum agree quite well with the simulations. Yet there appear to be two qualitative discrepancies in the figure. Near 3.6 Å, the experiment shows a double peak whereas the simulations only show a single peak. There is however a second peak in the simulation 0.05 Å below the one shown. We suppressed this second peak to improve visualization. Thus, the difference between simulation and experiment is not necessarily qualitative but perhaps only quantitative in nature.

In summary, it seems that all the three model potentials support the structure seen by Kingma. Still these results are questionable as the models were parametrized for ambient conditions and are not verified to reproduce the real behavior under such extreme pressures. Finding the transition path ways with ab initio might be too time consuming as the transition is only quasi-displacive, i.e., significant thermal activation is required although no bonds are destroyed. After α-quartz becomes unstable, several 1,000 MD steps have to be simulated before the new, stable structure is reached.

D. Stability of β-cristobalite

Quartz is not the only polymorph that is (meta) stable at ambient conditions. Cristobalite, a cubic polymorph, is found to be stable as well during accessible experimental time scales. [46, 47] A model potential that is used to mimic the behavior of silica should be able to reflect the experimentally observed stabilities. In some cases, the observation of stability in a simulation might be fortuitous as it could be the consequence of periodic boundary conditions and/or the number of atoms used. For example, the phase into which the system would like to convert is not compatible with the number of atoms used in the simulation or it cannot be accessed without a major reconstruction of the cell shape. This issue will be discussed in more detail in this section with a focus on cristobalite that shows significant effects depending on the choice of the periodic boundary conditions.

For the simulation of a crystalline system, the crystal structure has to be placed inside the box in a way that the periodic images fit to each other at the box ends. For the initial configuration of a simulation the atom positions are chosen to be identical with experimental crystallographic data such that the atoms were set onto ideal lattice positions and are equilibrated. For many systems and also for the case of cristobalite there are different ways to arrange such an initial configuration.

The most natural configuration is according to the usual description of cristobalite as a diamond structure for the silicon atoms with connecting oxygen atoms between each neighboring pair of silicon atoms. This would place the [100] crystal direction parallel to the z axis of the simulation box, and the box geometry would be cubic.

Alternatively, one can also use the ABCABC layering of sheets of hexagonal rings in the cristobalite structure, which is also a common representation as it leads to tridymite when the layers are stacked in an ABAB order. (To be precise, the silicon atoms are stacked as AABBAABB.) This layering is seen along the [111] direction in the crystal, and accordingly would place this direction parallel to the z axis of the simulation box when the layers are stacked in the xy plane.

Both geometries are completed by the periodic boundary conditions to form an infinite cristobalite crystal, and therefore they are equivalent regarding the static structure. However, the connectivity of the atoms at the boundary is different and therefore the two geometries do not sample equivalent lattice vibrations.

This difference becomes obvious in the simulation of β-cristobalite. When relaxing the BKS crystal at $T = 1273$ K and zero external pressure, where cristobalite is considered to be thermodynamically stable, [1] the volume of the simulation quickly stabilizes to a value close to the experimental value of $V_{SiO_2} = 45.25$ Å^3. In contrast with the second configuration, which had the [111] direction parallel to the z axis, the observed volume is, if at all, metastable only for a short period of time, before densification of the system takes place. After 2 ps the system is
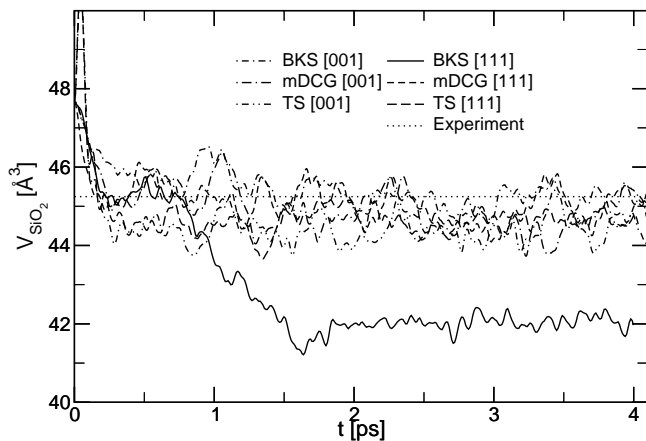
FIG. 8: Time evolution per SiO_2 unit V_{SiO_2} for the two geometries with three different potentials.
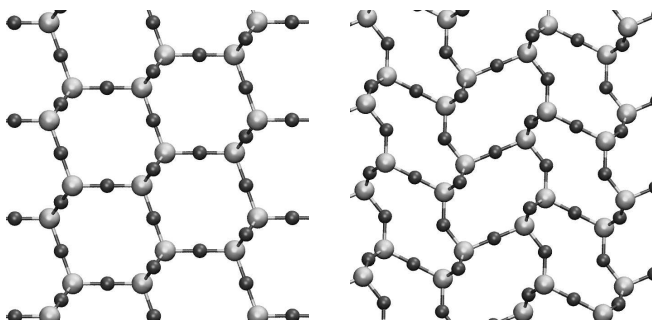

FIG. 9: Averaged structure as in the ideal cristobalite phase (left), which is stable in this configuration in mDCG and TS, and in the compressed phase (right) after a short simulation run with the BKS potential starting from the ABC setup.

FIG. 10: Volume per SiO_2 unit against temperature for the three different potentials with the cubic setup. Crosses denote experimental data in the α and the β-phase.
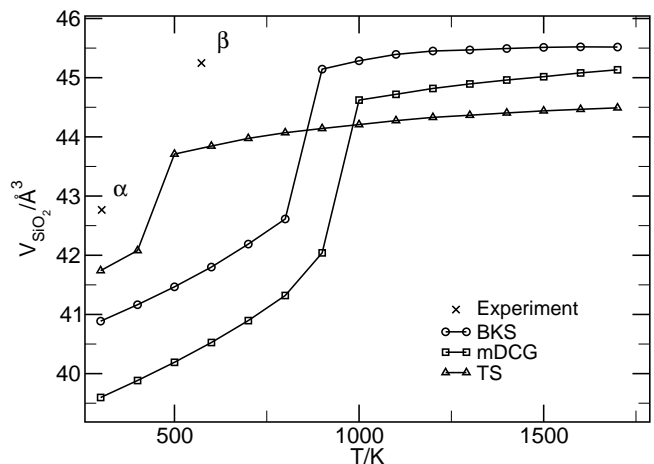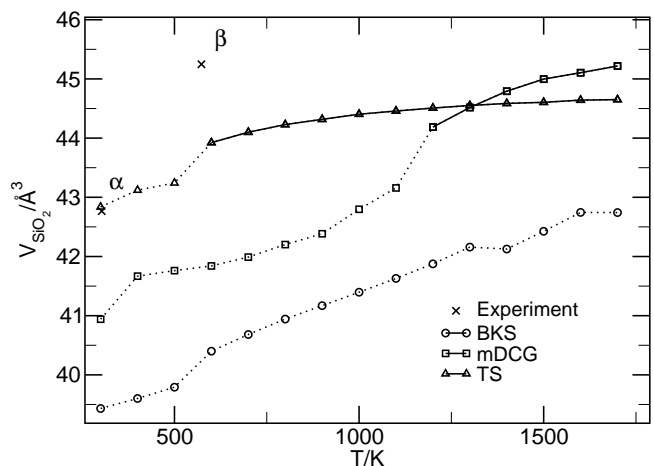

FIG. 11: Volume per SiO_2 unit against temperature for the three different potentials with the ABC setup. Crosses denote experimental data in the α and the β-phase. The dotted lines indicate non crystalline phases.

stable in a phase which is much denser than cristobalite. It was tested that this state remains stable for more than a nanosecond, which is not shown in the picture.

Obviously in contrast to this both the fluctuating charge and the fluctuating dipole potential do not exhibit such a behavior, but remain stable in the cristobalite phase regardless of the initial condition. Apparently the cristobalite phase is unstable in the BKS potential, but appears to be metastable if certain modes are prohibited by the periodic boundary conditions.

The examination over a larger temperature range yields a similar picture. Experimentally it is known that β-cristobalite undergoes a phase transition upon cooling to α-cristobalite, however, this transition is experimentally troublesome. Measurements for the transition temperature range from 393 K to 545 K. [1] The simulation results for the cubic setup as shown in Fig. 10 exhibit a far broader spread of transition temperatures, while the transition temperature for TS model agrees best with experiment. However the drawback for this model is that the transition is not reversible on the time scale of the simulation. Even though the α-phase is stable at low temperatures and rearranges to the β-phase above the transition point, the simulation would not find the α-phase by itself when cooling down β-cristobalite. The "artificial" phase has an energy that is only 10 K higher than that of α-cristobalite for classical systems at small temperatures. Given this small energy difference and given the smaller volume of the artificial phase, it may well be that the quantum-mechanical ground state energy adds significantly to favor α cristobalite over the artificial phase.

Fig. 11 shows the equation of state for the rotated system with the ABC setup. As seen above for a temperature of 1273 K, the disability of the BKS potential to form a stable β-cristobalite configuration with the ABC setup holds for the whole temperature range under consideration. Also for the mDCG potential the equation of state differs from the case of the cubic setup and shows only a small stability range for β-cristobalite as a com-
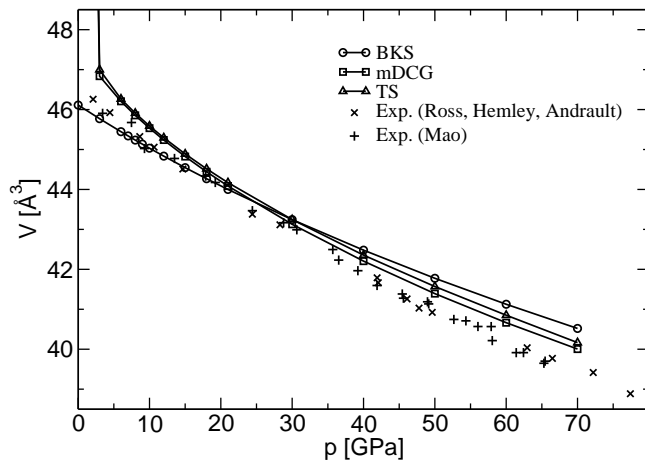
FIG. 12: Stishovite Equation of State. Solid circles are the data of Ross et al. [48], Hemley et al. [49], and Andrault et al. [50]; open squares are the data of Mao et al. [51]

FIG. 13: c/a ratio in stishovite against pressure. Experimental data as in Fig. 12. Note that the c/a and the volume are continuous at the phase transition from tetragonal to orthorhombic stishovite.

parison of figures 10 and 11 reveals. Only the results of the TS potential are essentially unaffected by the specific choice of how the cristobalite geometry is set up.

E. Stishovite

The quartz and cristobalite phases studied in this paper are composed of corner-sharing SiO_4 tetrahedra, which is the usual connectivity in the low-pressure phases. Stishovite in contrast is a polymorph that often serves as a prototype phase having octahedrally coordinated silicon. It is often assumed [25, 26] that with the fluctuating charge approach the ability of charges to adapt to the local configuration is especially helpful for the transferability between differently coordinated structures. It is also likely that the degree of ionicity changes with pressure. Therefore, one might expect that the fluctuating charge potential fits to the available experimental data best.

At room temperature, stishovite is stable for high pressures, i.e., above 8 GPa. It was also found to be metastable at ambient pressures. It was first synthesized in the laboratory [52] and later discovered in association with coesite. [53] Stishovite has the rutile structure, which consists of infinite chains of edge-shared SiO_6 octahedra parallel to the c-axis. Each oxygen atom is coordinated by three silicon atoms. [49]

The equation of state for stishovite under pressure is shown in Fig. 12. The agreement in the low pressure range is relatively good for the BKS potential, while neither the fluctuating dipole and nor the fluctuating charge potential produce a stable stishovite phase at zero pressure. When increasing the pressure, these two potentials constantly underestimate the density of stishovite, while the volume of the BKS simulation deviates more for higher pressures.
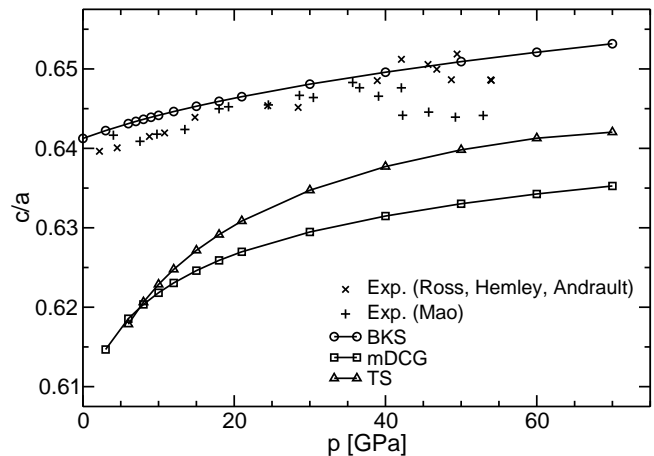
An interesting feature of stishovite under pressure is a different compressibility in the a and c direction, which is shown in Fig. 13. This plot shows again a very good agreement of the BKS data with the experimental results. The effect of the different compressibility in mDCG and TS is rather overestimated, while the TS potential again improves in the quantitative prediction for higher pressures. The result of the fluctuating charge potential shows no improvement over neither of the two other potentials.

1. High-Pressure Behavior

Shortly after the discovery of stishovite, a major question evolved around possible transformations to a denser structure at high pressures. Indeed, a pressure-induced phase transition near 50 GPa was suggested by crystal chemical arguments [54] and first-principle calculations, [55, 56] and later confirmed experimentally. [57–60]

At the transition, the SiO_6 octahedra are only slightly tilted, with the result that the lattice constants a and b, which are identical in the low pressure rutile-type, tetragonal phase, have different values in the $CaCl_2$-type orthorhombic stishovite. This tilting has the same symmetry as the stishovite B_{1g} vibrational mode, which was identified as the pressure-induced soft mode that drives the transition. [54] By means of a Landau expansion, Carpenter et al. [60] found a classical second-order character. The transition has almost no impact on the volume or the c/a ratio, which is shown in the paper by Carpenter.

However molecular dynamics models were not able to reproduce the transition pressure. They only found the transition at pressures in the megabar region. [13, 55, 61] As a comparison between molecular dynamics and experiment the elastic constants can be analyzed. Carpenter
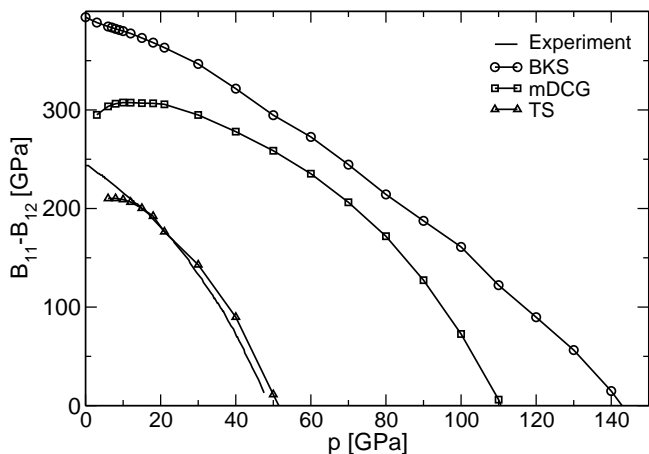
FIG. 14: Birch coefficients B_{11}-B_{12} as a function of pressure. Simulation data is compared to the result of a Landau expansion by Carpenter et al. [60]

FIG. 15: Lattice constants a and b against pressure. Experimental data as in Fig. 12.

et al. [60] used a Landau expansion to generate expressions for the elastic constants of stishovite with pressure. Fig. 14 shows the relevant shear modulus B_{11}-B_{12}, which softens on approach of the transition, as the B_{1g} mode directly contributes to it. The Birch coefficients B_{ij} have to be considered for a stability analysis rather than the elastic constants C_{ij}, when the system is observed under external pressure. [62] In the case of the two coefficients needed here, they are related to each other as $B_{11} = C_{11} - p$ and $B_{12} = C_{12} + p$.

One can see that the BKS potential and the fluctuating dipole potential show a softening towards pressures of over 100 GPa, which is in agreement to the molecular dynamics simulations cited above, and far away from the 50 GPa measured experimentally. In contrast the fluctuating dipole potential predicts the transition observed experimentally at 50 GPa [60] almost perfectly.

This prediction can be verified by plotting the lattice constants a and b, which coincide in a tetragonal lattice and differ in an orthorhombic lattice. In Fig. 15 the course of the lattice constants with pressure is compared to experimental data. The transition is clearly visible at a pressure of around 50 GPa in both the fluctuating-dipole simulation and experiment. The lattice constant is overestimated constantly in the simulation, which was already obvious from the results for the volume, see Fig. 12.

However the agreement with experiment in this phase transition is far better than in the other model potentials. This is rather surprising, as it was parametrized for tetrahedrally coordinated silicon only.

IV. CONCLUSIONS AND OUTLOOK

In this work, we compared three different model potentials for the simulation of pure silica. The model potential were a commonly used two-body potential parametrized by van Beest, Kramers, and van Santen (BKS), [4] a fluc-
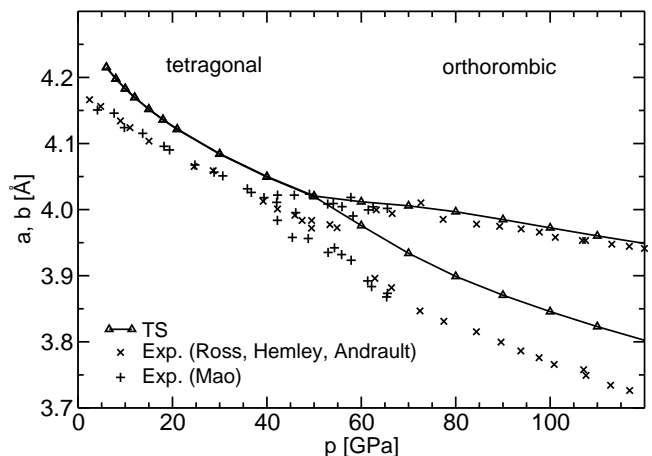
tuating charge potential, and a fluctuating dipole potential suggested by Tangney and Scandolo. [26] The fluctuating charge potential (mDCG) was a *modified* version of the energy surface proposed by Demiralp, Cagin, and Goddard such that it reflected the equation of state and $g(r)$ in α-quartz reasonably well. (Also later results by the same authors, stating "improved" values turned out to produce meaningless results in our runs, unlike the easily reproducible data on TiO_2 published in Refs. 30, 31.)

In the TS potential, the dipoles can adjust to the local electrical field and likewise the charges in the mDCG potential. Thus, these two approaches incorporate implicitly many-body interactions. The simulation results obtained with BKS, TS, and mDCG were compared to a large set of experimental data available for different SiO_2 polymorphs. Special attention was paid to those experiments that cannot be reflected satisfactorily with BKS. The mDCG potential leads - if at all - to an almost negligible improvement over BKS. The density of states (DOS) in α-quartz and the stability of β-cristobalite is slightly improved in mDCG with respect to BKS, but in some cases, i.e., the elasticity of β quartz or the c/a ratio in stishovite, BKS outperforms mDCG.

Conversely, the TS potential remedies all the qualitative failures of the BKS potential, including the c/a anomaly at the $\alpha - \beta$ transition in quartz, the DOS in α-quartz, the stability of cristobalite and tridymite, as well as the shape of the SiO_4 units in quartz at room temperature. Unfortunately, the TS potential only performs systematically better than BKS for polymorphs in which the silicon atoms are four coordinated. The pressure-induced transition from α-quartz to quartz II occurs at too high pressures using TS. Also the equation of state and the c/a ratio in stishovite is reproduced more satisfactorily with BKS than with TS. On the other hand, TS predicts the correct transition pressure P^* for the soft-mode driven second-order transition in stishovite, while BKS overestimates that value by more than 100%. In conclusion, one may recommend TS for simulations in

which tetrahedral SiO$_4$ units connect via corner sharing oxygen atoms.

We want to conclude our paper by commenting on some preliminary results on the piezoelectrical coefficients that one obtains with the TS potential. The details of this unfinished study will be discussed elsewhere, because many methodological points need to be addressed for the calculation of electro-mechanical coefficients. It seems as though TS reproduces piezoelectrical coefficients only well if the external electrical field is not coupled to the dipoles. This observation suggests that Tangney and Scandolo parametrized effects that are due to three-body interactions (or higher order) effectively into the dipole interactions. Indeed, we observe a large correlation between the magnitude of the dipoles and the Si-O-Si bond angle, which supports this suspicion. Thus, despite the significant improvements thanks to the TS potential, there is still room for further advancement in the construction of reliable model potential for silica and ultimately silicates. We hope that our study constitutes a reasonable reference check list for future examinations of SiO$_2$ model potentials.

[1] P. J. Heaney. Structure and chemistry of the low-pressure silica polymorphs. In P. J. Heaney, C. T. Prewitt, and G. V. Gibbs, editors, *Silica - Physical Behaviour, Geochemistry, and Materials Applications*, volume 29 of *Rev. Mineral.*, page 1. Mineral. Soc. of Am., Washington D. C., 1994.

[2] L. V. Woodcock, C. A. Angell, and P. Cheeseman. Molecular dynamics studies of the vitreous state: Simple ionic systems and silica. *J. Chem. Phys.*, 65:1565, 1976.

[3] S. Tsuneyuki, M. Tsukada, H. Aoki, and Matsui. *Phys. Rev. Lett.*, 61:869, 1988.

[4] B. van Beest, G. Kramer, and R. van Santen. *Phys. Rev. Lett.*, 64:1955, 1990.

[5] S. Tsuneyuki, H. Aoki, M. Tsukada, and Matsui. *Phys. Rev. Lett.*, 64:776, 1990.

[6] I. P. Swainson and M. T. Dove. *J. Phys. Cond. Matt.*, 7:1771, 1995.

[7] M. T. Dove, D. A. Kreen, A. C. Hannon, and I. P. Swainson. *Phys. Chem. Miner.*, 24:311, 1997.

[8] J. S. Tse and D. D. Klug. *Phys. Rev. Lett.*, 67:3559, 1991.

[9] J. S. Tse, D. D. Klug, and Y. Le Page. *Phys. Rev. B*, 46:5933, 1992.

[10] J. Badro, P. Gillet, and J.-L. Barrat. *Europhys. Lett.*, 42:643, 1998.

[11] J. S. Tse and D. D. Klug. *J. Chem. Phys.*, 95:9176, 1991.

[12] I. Saika-Voivod, F. Sciortino, T. Grande, and P. H. Poole. *Phys. Rev. E*, 70:061507, 2004.

[13] J. S. Tse, D. D. Klug, and Y. Le Page. *Phys. Rev. Lett.*, 69:3647, 1992.

[14] J. S. Tse, D. D. Klug, and Y. Le Page. *Phys. Rev. B*, 51:16392, 1995.

[15] J. Badro, D. M. Teter, R. T. Downs, P. Gillet R. J. Hemley, and J.-L. Barrat. *Phys. Rev. B*, 56:5797, 1997.

[16] J. Badro, J.-L. Barrat, and P. Gillet. *Phys. Rev. Lett.*, 76:772, 1996.

[17] K. Vollmayr, W. Kob, and K. Binder. *Phys. Rev. B*, 54:15808, 1996.

[18] S. N. Taraskin and S. R. Elliot. *Phys. Rev. B*, 56:8605, 1997.

[19] P. Jund and R. Jullien. *Phys. Rev. Lett.*, 83:2210, 1999.

[20] J. Horbach and W. Kob. *Phys. Rev. B*, 60:3169, 1999.

[21] J. Horbach and W. Kob. *Phys. Rev. E*, 64:041503, 2001.

[22] I. Saika-Voivod, P. H. Poole, and F. Sciortino. *Nature*, 412:514, 2001.

[23] M. H. Müser and K. Binder. *Phys. Chem. Miner.*, 28:746, 2001.

[24] M. Benoit and W. Kob. *Europhys. Lett.*, 60:269, 2002.

[25] E. Demiralp, T. Cagin, and W. A. Goddard III. *Phys. Rev. Lett.*, 82:1708, 1999.

[26] P. Tangney and S. Scandolo. *J. Chem. Phys.*, 117:8898, 2002.

[27] M. Hemmati M. Wilson, P. A. Madden and C. A. Angell. *Phys. Rev. Lett.*, 77:4023, 1996.

[28] A. Pasquarello and R. Car. *Phys. Rev. Lett.*, 79:1766, 1997.

[29] A. K. Rappé and W. A. Goddard III. *J. Phys. Chem.*, 95:3358, 1991.

[30] Varghese Swamy and Julian D. Gale. *Phys. Rev. B*, 62:5406, 2000.

[31] Varghese Swamy, Julian D. Gale, and l. S. Dubrovinsky. *J. Phys. Chem. Solids*, 62:887, 2001.

[32] M. Wilson and P. A. Madden. *J. Phys.: Condens. Matt.*, 5:2687, 1993.

[33] H. Schober, D. Strauch, K. Nützel, and B. Dorner. *J. Phys: Cond. Mat.*, 5:6155, 1993.

[34] G. Roma, Y. Limoge, and S. Baroni. *Phys. Rev. Lett.*, 86:4564, 2001.

[35] F. Galeener. *Phys. Rev. B*, 19:4292, 1979.

[36] A. Pasquarello and R. Car. *Phys. Rev. Lett.*, 80:5145, 1998.

[37] D. L. Price and J. M. Carpenter. *J. Non-Cryst. Solids*, 92:153, 1987.

[38] M. A. Carpenter, E. K. H. Salje, A. Graeme-Barber, B. Wrucki, M. T. Dove, and K. S. Knight. *Am. Mineral.*, 83:2, 1998.

[39] K. Binder. *Phys. Rev. Lett.*, 47:693, 1981.

[40] H. Grimm and B. Dorner. *J. Phys. Chem. Solids*, 36:407, 1975.

[41] G. S. Smith. *Acta Cryst.*, 16:542, 1963.

[42] K. Kihara. *Eur. J. Miner.*, 2:63, 1990.

[43] J. Tse, D. D. Klug, Y. Le Page, and M. Bernasconi. *Phys. Rev. B.*, 56:10878, 1997.

[44] C. Campaña, M. H. Müser, J. S. Tse, D. Herzbach, and P. Schöffel. *Phys. Rev. B*, 70:224101, 2004.

[45] K. J. Kingma, R. J. Hemley, H. K. Mao, and D. R. Veblen. *Phys. Rev. Lett.*, 70:3927, 1993.

[46] J. B. Jones and E. R. Segnit. *J. Geol. Soc. Australia*, 18:419, 1972.

[47] W. A. Dollase. *Acta Cryst.*, 23:617, 1967.

[48] N. L. Ross, J. F. Shu, and R. M. Hazen. *Am. Min.*, 75:739, 1990.

[49] R. J. Hemley, C. T. Prewitt, and K. J. Kingma. High-pressure behaviour of silica. In P. J. Heaney, C. T. Prewitt, and G. V. Gibbs, editors, *Silica - Physical Behaviour, Geochemistry, and Materials Applications*, volume 29 of *Rev. Mineral.*, page 41. Mineral. Soc. of Am., Washington D. C., 1994.

[50] D. Andrault, G. Fiquet, F. Guyot, and M. Hanfland. *Science*, 282:720, 1998.

[51] H. K. Mao, J. Shu, J. Hu, and R. J. Hemley. *Eos Trans. AGO, Fall Meet. Suppl.*, 75(44):662, 1994.

[52] S. M. Stishov and S. V. Popova. *Geochem. (USSR)*, 10:923, 1961.

[53] E. C. T. Chao, J. J. Fahey, J. Littler, and D. J. Milton. *J. Geophys. Res.*, 67:419, 1962.

[54] L. Nagel and M. O'Keeffe. *Mater. Res. Bull.*, 6:1317, 1971.

[55] R. J. Hemley, M. D. Jackson, and R. G. Gordon. *Eos Trans. AGU*, 66:357, 1985.

[56] R. E. Cohen. *Geophys. Res. Lett.*, 14:37, 1987.

[57] R. J. Hemley. Pressure dependence of raman spectra in sio$_2$ polymorphs: α-quartz, coesite, and stishovite. In M. H. Manghnani and Y. Syono, editors, *High Pressure Research in Mineral Physics*, volume 39 of *Geophys. Monogr. Ser.*, page 347. AGU, Washington D. C., 1987.

[58] Y. Tsuchida and T. Yagi. *Nature*, 340:217, 1989.

[59] K. J. Kingma, R. E. Cohen, R. J. Hemley, and H. K. Mao. *Nature*, 374:243, 1995.

[60] M. A. Carpenter, R. J. Hemley, and Ho kwang Mao. *J. Geophys. Res.*, 105:10807, 2000.

[61] D. J. Lacks and R. G. Gordon. *J. Geophys. Res.*, 98:22147, 1993.

[62] D. C. Wallace. *Thermodynamics of Crystals*. Wiley, New York, 1972.